Evidence for Planet Nine with a 3,600-Year Period and 1 AU Perihelion as the Cause of Recurring Apocalypses

Pavlo Kandyba / pavlonlo83@gmail.com

March 1, 2026

Abstract

A model of Planet Nine (P9) as a massive body (5 $M_\oplus$) in a highly eccentric retrograde orbit ($e \approx 0.994$–0.996, $q \approx 1$ AU, $Q \approx 400$–500 AU, $T \approx 3600$ yr), presumably captured from interstellar space. The model relies on the clustering of ETNO orbits by alignment with P9. It also shows quasi-periodicity in climatic and cultural-historical markers (the Younger Dryas event, the Piora oscillation) consistent with a period of $T \approx 3600$ yr. A historically confirmed possible observation of Planet Nine's perihelion passage of 1 AU has been established, supported by the exploratory LLM reconstruction of the comet's orbit observed in CE 60 for 180 days and documented in Chinese chronicles. Numerical simulations have shown relative orbital stability over a period of about 1000,000 years.

1 Introduction

The hypothesis of Planet Nine (P9), a massive undiscovered planet in the outer Solar System, was initially proposed to explain the clustering of orbits of distant trans-Neptunian objects with semimajor axes $a > 250$ AU (Batygin & Brown, 2016).

Subsequent refinements constrained its parameters to a semimajor axis of 290 ± 30 AU, eccentricity $e \approx 0.29$, and mass $4.4 \pm 0.4\ M_\oplus$ (Siraj et al., 2025).

However, alternative origins have been explored in simulations, such as capture from interstellar space as a rogue planet, yielding capture probabilities of 0.05–40% under certain conditions (Vesper & Mason, 2017; Mustill et al., 2016).

It is assumed here that P9 may occupy a highly eccentric ($e \approx 1.0$) retrograde orbit with $q \approx 1$ AU and $Q = 300$–500 AU, captured relatively recently.

Orbital dynamics of ETNO clustering by an aligned high-eccentricity P9 orbit are dominated by orbit-averaged perturbations, leading to a stable fixed point in the phase space of angular elements.

The secular Hamiltonian admits equilibrium solutions characterized by libration of the longitude of perihelion,

$$\Delta\varpi = \varpi_{\mathrm{ETNO}} - \varpi_{\mathrm{P9}} \approx \pi,$$

which results in long-lived anti-alignment of ETNO perihelia with respect to P9. Simultaneous libration of Ω and ω constrains the orientation of ETNO orbital planes, producing a three-dimensional clustered configuration.

For highly eccentric perturbers, retrograde configurations expand the domain of secular stability by reducing resonance overlap and suppressing chaotic diffusion. As a result, a retrograde, near-parabolic P9 orbit can sustain coherent clustering of ETNO angular elements over Myr timescales despite strong perihelion penetration into the inner Solar System (Kandyba 2024).

In this maximally apocalyptic scenario, P9 impulsively and chaotically interacts with the inner Solar System, potentially entraining a trail of small bodies, meteoroids, and dust clouds from the Kuiper Belt. This exerts quasi-cyclic influence on the planets of the Solar System, including Earth. The gravitational influence of P9 also implies an impact on solar activity, which significantly contributes to climate (Hung, 2007).

This hypothesis explicitly rejects the assumption that the current orbital configuration of Planet Nine represents a long-lived solution. Instead, it is considered the Solar System as a time-dependent dynamic system, currently observed in a transitional, metastable state.

This naturally explains why the presumed orbital properties of extreme trans-Neptunian objects appear dynamically unstable and sensitive to sample selection.

N-body studies of massive bodies on high-eccentricity orbits intersecting planets show that orbital energy diffusion occurs on timescales of (10^2–10^3) perihelion passages.

1–3 million years ago, the Mid-Pleistocene Transition occurred from a 41,000-year to a 100,000-year cycle, corresponding to the main cycle of eccentricity changes (Clark et al., 2006). This "Transition Problem" requires explanation. Accordingly, hypotheses establish a strict upper limit ($\sim$1–3) million years in the past for the current orbital configuration.

2 Goals and Objectives

To test this model, based on historical data, I'm attempt to find traces of flybys and determine a quasi-cycle indicating the orbital period of P9.

The key assumption is as follows:

Each orbital cycle of P9 is not necessarily accompanied by a catastrophe; the impact of P9 is often realized through a trail rather than direct close approach.

Possible flyby scenarios also include passage at a safe distance and shielding by the Sun. Consequently, the absence of geological markers does not imply the absence of a flyby. This makes the search for strict periodicity in geology fundamentally impossible. From this follows a methodological conclusion: geological markers cannot be the sole source for identifying the quasi-cycle.

To compensate for the incompleteness of the geological record, I'm expand the observational space and introduce cultural-historical markers: religious dates, mythological plots, prophecies, cosmogonic cycles and ancient astronomical observations.

Each of the three aspects—astronomical, geological, and cultural-historical—I'm, first consider separately, then compare statistically and qualitatively to search for correlations or coincidences.

3 Characteristics of Planet Nine's Orbit

Here, I adopt a strict constraint $q \approx 1$ AU and aphelion in the range $Q \approx 300$–500 AU. This scenario, implying intersection with Earth's orbit, is of utmost importance to, and the primarily aim to exclude or confirm it. It also hypothetically allows to attempt to track the orbital period of P9 within the relative accuracy of event dating.

The resulting semimajor axis lies between $a = 150.5$ and 250.5 AU. By Kepler's third law, this corresponds to orbital periods in the range $T \approx 1.8$–4.0 kyr, with eccentricities $e \approx 0.993$–0.996. Thus, millennial-scale periods arise naturally from the imposed geometric constraints, without additional assumptions. This yields a period $T \approx 1,800$–$4,000$ years.

At $q = 1.0$ AU, the object intersects the orbits of all terrestrial planets, but the inclination of its orbit relative to the plane of the ecliptic is allowed. The high frequency of Kuiper Belt crossings combined with planetary mass causes massive injection of small bodies into the inner system, forming quasi-cyclic "epochs of impact chaos." In this case, the noise resulting from scattering is suppressed by the fact that most of the objects are retained by the giant planets and only a small amount penetrates into the inner part Solar System, contacting P9 as a conductor during its perihelion passage.

It is worth noting that at such extreme eccentricity, the object spends the overwhelming majority of its time near aphelion. The parameters closely resemble those of hypothetical objects predicted within the "Planet Nine" hypothesis or extreme trans-Neptunian objects (ETNOs).

4 Astronomical Events in Ancient Myths and Historical Chronicles

4.1 Background to the Study

Astronomical events in ancient myths are of undeniable interest. In conditions where object passages may be accompanied only by optical effects, weak gravitational influence, or local meteor episodes, a significant portion of orbital cycles remains geophysically invisible.

In such a situation, historical-cultural and mythological sources are considered as an independent archive of observations, recording stable astronomical motifs. Human culture is a resonant accumulator of anomalies, which well remembers

what is rare, incomprehensible, and does not fit into habitual classifications.

Thus, the involvement of mythological and religious traditions in this work is a necessary methodological step aimed at compensating for the incompleteness of geophysical data and testing the hypothesis of orbital cyclicity on the broadest, independent material.

For the selected period, I'm choose three astronomically saturated culmination points of history: Göbekli Tepe, Sumer, and the Beginning of the New Era.

4.2 Göbekli Tepe

The earliest period likely associated with the fixation of astronomical events is the time before the start of construction of the oldest temple complex Göbekli Tepe, dated approximately 9600–9000 BCE. In astronomical interpretation, it depicts presumed constellations (Sweatman & Tsikritsis, 2017):

Vulture / Eagle: constellation Sagittarius.

Scorpion: constellation Scorpius.

Leaping crane: constellation Cygnus or Aquarius.

Wolf / Dog: constellation Lupus.

Relation to solstice and equinox points, presumably depicted as four bags, in modeling gives the most precise match at 10,950 (±250) BCE.

This is linked to the YDIH (10,800 BCE), the presumed disintegration of Comet Encke, and the formation of the Taurid meteor stream.

On many pillars of Göbekli Tepe, streams of snakes moving downward are depicted. In astronomical interpretation, these are bolides formed as a result of comet disintegration near its perihelion, when Earth collided with its tail.

In 10,950 BCE, at the moment of summer solstice, the Sun was on the border of Sagittarius and Scorpius near the Galactic Center. Today, due to precession, the summer solstice point has shifted nearly 180 degrees and is now in the constellation Taurus on the border with Gemini.

Additionally, according to Plato, the final flooding of Atlantis occurred 9600 BCE, coinciding with the end of the Younger Dryas and the time of Göbekli Tepe's foundation.

I'm assume, that the temple complex could have been founded in honor of a series of events caused by P9.

4.3 Sumer

The subsequent millennia do not contain brightly expressed astronomical cultural markers until the period of the urban revolution, the emergence of writing, and developed astronomy in Sumer in the period 4000–3000 BCE.

At this time, the earliest evidence of the emergence of Sumerian mythology appears (3100–2900 BCE) and the first mention of Marduk (2800–2600 BCE)—the main hero of the famous cosmogony "Enuma Elish," in which the creation of the world occurs through the destruction of the old order.

The catastrophic events described in it are often linked both to the YDIH (10,800 BCE), the presumed disintegration of Comet Encke, and to Earth's re-entry into its debris trail, the Taurid stream (peak density 3200 BCE).

Possibly, Enuma Elish simultaneously describes both these events. The continuity of bag symbols from Göbekli Tepe to the Sumerians may indirectly testify to this. The collapse of the Uruk period in Mesopotamia is linked to the peak of the Piora Oscillation, which possibly contributed to myths of floods in Babylonian and Biblical folklore.

In Enuma Elish, the destroyer god Marduk appears before us in an image consonant with the description of a cometary body forming a coma and tail into which Earth fell:

"He flashed lightning before him,
He filled his body with blazing flame."

and

"He released before him the Evil Wind, which was behind him."

Enuma Elish also hints at cyclicity:

"He returned to Tiamat, whom he had vanquished."

It was during the period of the presumed repeated return of Comet Encke that the world order of Sumerian civilization attributed to Marduk was established.

In MUL.APIN, the earliest systematic astronomical compendium of Babylon (∼1000 BCE), a direct and unambiguous identification of Marduk with Jupiter is given:

"The star of Marduk, Nēbiru, Jupiter."

Where Nēbiru means "crossing," "transition" across the celestial equator.

This accurately describes Jupiter's behavior but poorly aligns with the description of Marduk in Enuma Elish as a tailed destroyer. And we pose the question—is this not an identification of Jupiter itself with another, unobserved but historically traced object?

In some Babylonian astronomical texts, there is mention of a star's color:

"In the month Du'uzu [June-July], when the Star of the Arrow [Sirius] shines, ... a great star, whose color is red, like copper, divides the sky in half. This is Nibiru."

and

"A brown-red star... divides the heavens and stands there, this star—Nebiru-Marduk."

This is likely related to atmospheric conditions but may also be a reference to real Marduk, the object described in the myth.

In Greek mythology, Typhon, a monster that went against the gods, was described as a celestial body moving unnaturally and causing storms. He corresponds to Seth in Egyptian mythology.

Nonnus describes Typhon as a celestial aggressor who attacks the constellations themselves and changes their course.

Pliny the Elder, in his Natural History (Book 2, sections on comets and winds, around chapters 22–23 and 49), directly links Typhon to an astronomical phenomenon, calling it a "fiery whirlwind":

"The ancients mention a comet which they called Typhon... it was of bloody color and had the appearance of a circle, twisted like a whirlwind, and its sight inspired terror; it was not a star, but rather some fiery knot."

"A terrible comet was seen by the people of Ethiopia and Egypt, to which Typhon the king of that period gave his name; it had a fiery appearance and was twisted like a coil, and it was very grim to behold: it was not really a star so much as what might be called a ball of fire."

"When such bodies appear, they portend great droughts, followed by huge floods."

Joannes Lydus referring in "De ostentis" to other authors, adds a detail about the northern location (Clube;Napier 1982):

≪They say that the sixth comet is called 'Typhon' after the name of king Typhon, seeing that it was once seen in Egypt and which is said to be not a fiery but a blood-red colour. Its globe is said to be modest and swollen and it is said to have been for some time in the north. The Ethiopians and Persians are said to have seen this comet and suffered all evils and famine.≫

This description fully corresponds to the description of Marduk in Enuma Elish:

"He fashioned the Evil Wind, the Dust Storm, Tempest, The Four-fold Wind, the Seven-fold Wind, the Whirlwind,
And the wind which had no equal.

The Lord raised the Deluge, his mighty weapon.
He mounted the fearsome chariot of the irresistible storm-winds."

And therefore, we assume that Babylonian texts are an attempt to identify observed astronomical objects with the legendary.

4.4 Star of Bethlehem and Other Astronomical Prophecies

In the religious tradition, the Star of Bethlehem is a predicted event.

Prophet Balaam (Numbers 24:17):

"I see Him, but not now; I behold Him, but not near. A star rises from Jacob and a scepter rises from Israel..."

We assume that the prophet could have spoken about an event whose periodicity was known, and which should stand out against the background of others.

Jesus Christ or other people could study the scriptures and could have been familiar with astronomical and cosmogonic texts describing the cyclic appearance of cosmic objects. Identifying himself with the heavenly deity and describing his heavenly kingdom and army, Jesus spoke of his return as follows:

Gospel of Matthew, chapter 24 (Synodal translation):

27 "...for as lightning comes from the east and is visible even to the west, so will be the coming of the Son of Man..." 29 "And immediately after the tribulation of those days the sun will be darkened, and the moon will not give its light, and the stars will fall from heaven, and the powers of the heavens will be shaken..." 30 "...then will appear the sign of the Son of Man in heaven; and then all the tribes of the earth will mourn and see the Son of Man coming on the clouds of heaven with power and great glory."

The consonance of the Revelation of John the Theologian with Enuma Elish seems obvious — four winds, four horsemen, etc. Also about the return (Revelation 22:12):

"And, behold, I come quickly; and my reward is with me"

Apocryphal texts contain additional, possibly borrowed from more ancient ones as often happens, details:

Apocalypse of Peter (Ethiopian version)

Chapter 1:

5 "...Seven times brighter than the sun I will shine."

Chapter 5:

1 "...fiery waterfalls will pour, darkness and gloom will come and clothe and envelop the whole world, and waters will turn into burning coals, and everything on earth will burn, and the sea will become fire, and under heaven will be a cruel flame which will not be extinguished, but will rush to the judgment of wrath."

2 "And the stars will be scattered by the fiery flame, as if they had not been created, and the firmaments of the heavens will pass away for lack of water and become as uncreated." 3 "And there will be lightnings in heaven, and their sorcery will frighten the world."

These words echo the apocalyptic text of Enuma Elish, in some measure are confirmed by historical data (YDIH) and agree well with our hypothesis. Possibly they in distorted form describe events of the past.

5 Ancient Astronomical Observations

5.1 Astronomical Observations around 1 CE

The turning point of temporal epochs was marked by a whole series of documented astronomical and potentially astronomical events within about a hundred years against the background of another cultural shift, though not associated with global cataclysms.

We admit that the Star of Bethlehem can be seen rather as a symbol of the era of messianic expectations, and any event could be taken for this object.

We screen out confirmed events, and after filtering, unique ones remain that do not match the behavior of any known periodic comet and have no confirmed supernova remnants:

48 BCE — Ke-xing ("guest star") Duration: Several weeks Characteristics: In the area of Aquila Sources: Hanshu (or related chronicles); Pankenier (2013) notes it as an unidentified object

44 BCE Sidus Iulium (Caesar's Star) This is perhaps the most documented object of Rome. (Pliny the Elder, Natural History).

5 BCE — Comet (huixing, "broom star") Duration: ¿70 days Characteristics: Appeared in Qian-niu (area of Capricornus) Sources: Qian Han Shu (Hanshu), ch. 26, Tianwen Zhi (2nd year of Jianping, 2nd month ≈ March 9 – April 7, 5 BCE). This object is considered the main candidate for the Star of Bethlehem. New models of 2025 show the possibility of "hanging" over Bethlehem in June 5 BCE with a very close flyby (Matney, 2025).

4 BCE (April 24) — Bo-xing ("bushy star") Duration: Not specified (separate event) Characteristics: In He-gu (area of Aquila: Altair and neighboring stars) Sources: Hanshu, ch. 11 (day ji-yu); parallel Chinese/Korean records

35 CE — Comet (huixing, "broom star") Duration: Short (not specified) Characteristics: Broke into pieces (described as an ill omen) Sources: Hou Han Shu (early Eastern Han period)

39 CE — Comet Duration: Short Characteristics: Brief comet of the early Eastern Han period Sources: Hou Han Shu (compiled in the 5th century CE)

5.2 Cometary Activity During 54–68 CE

The reign of Nero (54–68 CE) stands out in ancient astronomical records due to an unusually high number of documented cometary apparitions, which were interpreted as omens amid political turmoil (Ramsey, 2006; Barrett, 2015). This period, marked by enhanced observational practices in both Roman and Chinese contexts, features at least four confirmed comets, with additional candidates, reflecting a convergence of scientific interest and superstitious dread (Ho, 1962; Kronk, 1999). Roman sources, such as Seneca and Tacitus, often linked these events to Nero's tyranny, while Chinese annals provided precise astronomical details.

5.3 Overview of Comets During 54–68 CE

54 CE: Appeared shortly after Claudius' death and Nero's accession (October 13, 54 CE); described as having a "bushy" tail and interpreted as a portent of regime change (Seneca, Naturales Quaestiones 7.17.2; Suetonius, Nero 8; Kronk, 1999).

60 CE (Comet C/60 D1): Visible from late November for approximately 135–180 days; the most prominent and longest-lasting of the period, detailed below (Seneca, Naturales Quaestiones 7.21.3; Ho, 1962; Ramsey, 2006).

64 CE: Observed from May to July, shortly after the Great Fire of Rome (July 18–27, 64 CE); noted as an "terrifying spectacle" amid accusations against Nero (Tacitus, Annals 15.47; Seneca, Naturales Quaestiones 7; Kronk, 1999).

66 CE (Comet 1P/Halley): Appeared January 31, lasting about 50–70 days; described as a "sword-like star" during the First Jewish-Roman War, with high brightness and cultural impact (Josephus, Jewish War 6.5.3; Ho, 1962; Kronk, 1999).

This cluster of comets, amplified by contemporaneous records, underscores the intersection of astronomy and imperial anxiety in the first century CE (Stephenson, 2002).

We think that such a peak in comet activity corresponds to the eras of chaos in connection with the flyby of P9, as predicted by this hypothesis.

5.4 Calculation of a Cycle Based on Historical and Cultural Events

When calculating a period based on historical and cultural events, hypothetically or directly related to astronomical events, the following statement is accepted:

1. Göbekli Tepe (GT) 10 950 BCE (±250 yr) is assumed to be the most accurate result of the reconstruction of a hypothetical astronomical event and remains fixed.

2. Emergence of Sumerian Mythology ∼3000 (∼3100–2900) BCE could have happened after the event and is not an exact date, so drift is possible.

3. Cometary Peak (CP) ∼60 CE is a precise historically documented date.

4. The event may be missed.

The result is obvious:

10 950 (GT) + 60 (CP) = 11 010 : 3 = 3670

Which is approximately equal to 3600, the legendary Sumerian mythological cycle Šár, used in the King List and approaches a multiple of 365–366 days a year. This "magic of numbers" is amazing because each number relates to an exceptional historical period, but proof requires more reliable proxy data.

6 Geological Constraints and the Quasi-Cyclic Nature of Rare Cosmic Impacts

In the past, Earth and the Solar System have experienced many catastrophic events that can be interpreted within this model. However, due to dating complexities and data incompleteness, this presents a very difficult task.

The aggregate of geological, geochemical, and climatic data from the past indicates a complex, nonlinear character of external and internal perturbations to Earth's climate system. Most of these processes are well explained by the internal dynamics of Earth's climate system, including degradation of ice sheets and redistribution of ocean circulation, and do not require invoking an external impact mechanism.

Therefore, I'm focus on events that are more likely to require a external forcing and take a time interval up to 15 000 BCE to enable tracking several cycles while maintaining relative dating accuracy.

I'm screen out all geophysical, climatic, confirmed impact events that stand out against the background of long-period climatic cycles, and in the period from 15 000 BCE to the present day, I'm identify three events meeting hypotheses requirements—the Younger Dryas Impact Event (YDIE), Piora Oscillation (PO) and Roman Climatic Optimum (RCO).

6.1 Younger Dryas Impact Event

The Younger Dryas is a sharp climatic episode of reverse cooling that occurred approximately in 10 900–10 800 BCE (start). This event interrupted the general warming during the transition from the Last Glacial Maximum to the Holocene, returning conditions in the Northern Hemisphere nearly to glacial values.

The Younger Dryas Impact Hypothesis (YDIH), proposing the disintegration of Comet Encke, is one of the most debated topics in modern geology and paleontology (Firestone et al., 2007). The essence of the hypothesis is that about 12,900 years BP, an airburst or collision with fragments of a large comet or asteroid occurred over North America. This event served as a trigger for abrupt cooling and catastrophic biosphere changes.

In sedimentary rocks of that period, magnetic microspherules and nanodiamonds have been found, which form only at ultra-high temperatures and pressures characteristic of cosmic body collisions.

Elevated concentrations of iridium and platinum—elements rare in Earth's crust but common in meteorites—were discovered. Extensive soot deposits indicate global forest fires that could have covered up to 10% of the land surface. According to this model, the impact triggered a chain reaction: striking the Laurentide Ice Sheet caused instantaneous melting of huge ice masses, ocean freshening, and megafauna extinction.

In my model, this event may be associated with a period of impact chaos caused by P9, and Comet Encke is a typical KBO ejected by it.

6.2 Piora Oscillation

From 4000–3000 BCE, a storm of climatic shifts and possible cosmic incidents occurred. In 3800–3600 BCE (Wick & Tinner, 1997), the Piora Oscillation began—a cooling with a peak around 3250–3150 BCE, a sharply onset cold and humid period in Holocene climatic history. The causes of its onset remain a subject of debate in paleoclimatology.

The end of the African Humid Period and the onset of Sahara aridization are dated to ∼3500–3800 BCE in some syntheses, correlating with the early phase of the Piora. In the Middle East, the Dead Sea level rose by 30 meters and then fell to near-modern levels. In Greenland ice cores, increases in methane and sulfate levels around 3250 BCE are visible, indicating a catastrophe—either a volcanic eruption or a meteorite or asteroid fall.

According to the "comet swarm" hypothesis (Encke–Taurid complex), developed by V. Clube, B. Napier, and other researchers, in the late 5th–early 4th millennium BCE, Earth may have experienced a series of catastrophic impacts associated with the disintegration of a giant comet, the progenitor of the modern Comet Encke (Clube & Napier, 1984; Napier, 2010).

These dates do not directly relate to the initial comet disintegration, which occurred much earlier. However, they fall within periods of possible peaks in Taurid complex activity on ∼3000-year cycles. In the Clube and Napier hypothesis, series of impacts or meteor bombardments associated with comet fragments could have occurred in the 4th millennium BCE (approximately 4000–3000 BCE).

There are groupings of objects indicating a possible peak flux around 3200 BCE. The Taurid orbit is highly evolved and degrading. However, in this period, there are no unambiguous traces of large-scale impact events.

The observed set of features allows an alternative interpretation in which P9 is the source of heterogeneous impact, such as gravitational impulse, its delayed consequences, captured material in the Kuiper Belt against the background of natural climatic shifts. This geophysical factors demonstrate clustering of extreme events consistent with the influence of one long-period external factor.

6.3 Roman Climate Optimum (RCO)

The Roman Climate Optimum (RCO; ca. 250 BCE–400 CE) represents an anomalous climatic state within the Holocene, distinguished by its exceptional **duration (≈4–6 centuries), low interdecadal variability, and broad regional coherence** (McCormick et al., 2012; Büntgen et al., 2011).

Crucially, the RCO does not align coherently with known solar cycles (11-yr Schwabe, 88-yr Gleissberg, ∼208-yr de Vries, or millennial-scale variability). Cosmogenic isotope records (^{14}C, ^{10}Be) suggest only moderate solar activity without a sustained multi-centennial maximum, and the amplitude of reconstructed solar forcing (∼0.1–0.3 W m^{-2}) is insufficient to maintain such a

long-lived warm regime on its own (Steinhilber et al., 2012; Gray et al., 2010).

No single dominant forcing—solar, volcanic, orbital, or greenhouse gas—adequately accounts for the magnitude, coherence, and persistence of the RCO. This has led to increasing recognition that some form of external forcing or triggering impulse, potentially short-lived but systemically amplified through internal feedbacks, may be required to explain the RCO's emergence and longevity (Marcott et al., 2013; Steinhilber et al., 2012).

Against this background, an event that occurred close to the middle of this period stands out. The early first-century CE interval along the Dead Sea Transform (DST) fault system is characterized as a seismic storm, marked by an anomalous cluster of earthquakes with magnitudes exceeding 6.0, occurring within a compressed 20–50-year window, contrasting sharply with the preceding and subsequent centuries' average recurrence intervals of 100–300 years for comparable events (Ben-Menahem, 1991).

Paleoseismic records from lacustrine varves and sediment cores at Ein Gedi and Ze'elim reveal intensified deformation layers, indicating a 2–3-fold increase in seismic energy release compared to the late Holocene baseline, with sparse activity in the first century BCE (e.g., one major event in 31 BCE) and a relative quiescence post-70 CE until the second century (Kagan et al., 2011; Williams, 2012).

The peak seismic activity along the DST (centered ∼31 CE ±5 yr) was abrupt and sharply defined, manifesting as a prominent seismite with a sharp upper contact in lacustrine cores (Ein Gedi, Ze'elim), indicating a sudden, high-intensity deformation event or brief cluster rather than gradual accumulation (Migowski et al., 2004; Williams, 2012). This contrasts with the nonperiodic, clustered Holocene pattern of the DST, where interevent times vary widely but lack such concentrated energy release in comparable short windows (Kagan et al., 2011; Wechsler et al., 2014).

This is consistent with model in which P9 may be a trigger for the Earth's internal dynamics.

6.4 Calculating the Period Based on Geophysical Events

The randomness of a close passage of a cosmic object directly near Earth and a very limited selection does not allow to attempt to determine the cycle based on these events; but when compared with the first number obtained (3670 yr), it gives a match:

10 900–10 800 BCE (central value ∼10 850 BCE), 3700 BCE (range 3800–3600 BCE), 31 CE.

Assuming these events are separated by integer multiples of an orbital period (P) in the approximate range 2000–4000 yr, the inter-event intervals are:

$\Delta t_1 \approx 7150$ yr (± 150 yr), $\Delta t_2 \approx 3731$ yr (± 100 yr).

The ratio

$\Delta t_1 / \Delta t_2 \approx 1.916$

is closest to the rational approximation 2/1. For multiplicity $k = 2$, $m = 1$

the condition

$\Delta t_1 = 2P \quad$ and $\quad \Delta t_2 = P$

yields $P = \Delta t_2$.

Solving within the dating uncertainties gives the consistent period range:

$P = 3631$–3644 yr (with central value ≈ 3638 yr), which is close to 3670 yr, received earlier.

7 Resonance Analysis of Solar and Climatic Cycles Relative to a 3600-Year Period

To rule out a simple coincidence, I correlate the resulting period (rounding up to 3600) with solar and climatic cycles. Periodic perihelion passages of our hypothetical P9 on a highly elliptical orbit could theoretically cause gravitational perturbations. Short-term tidal effects on Earth could change the orbital eccentricity or inclination, indirectly modulating Milankovitch cycles and causing climate shifts such as Heinrich events through enhanced iceberg calving or AMOC disturbances.

For each established solar or climatic cycle with period T_i, is determined the dimensionless ratio:

$$n_i = \frac{T_0}{T_i}. \tag{1}$$

A resonance is considered significant when n_i is close to a rational number with a small denominator:

$$\left| n_i - \frac{p}{q} \right| < 0.02, \tag{2}$$

where p and q are integers and $q \leq 3$. This criterion corresponds to a mismatch of less than ∼2%, consistent with uncertainties in paleoclimate and solar reconstructions (Bond et al., 2001; Usoskin, 2017).

Resonance types are classified as follows:

- Direct harmonic resonance ($q = 1$);
- Parametric (subharmonic) resonance ($q = 2$);
- Quasi-resonance ($q = 3$).

7.1 7.1. Solar Cycles: Resonance Relations

The analysis yields the following resonance relationships between T_0 and well-known solar variability modes:

- Schwabe cycle (∼11.1 yr): $T_0/T_i \approx 325 \rightarrow$ no resonance.
- Hale magnetic cycle (∼22.1 yr): $T_0/T_i \approx 163 \rightarrow$ no resonance.
- Gleissberg cycle (∼87 yr): $T_0/T_i \approx 41.4 \approx 124/3 \rightarrow$ weak quasi-resonance.
- de Vries (Suess) cycle (∼208 yr): $T_0/T_i \approx 17.3 \approx 52/3 \rightarrow$ quasi-resonance.
- Eddy cycle (∼1000 yr): $T_0/T_i = 3.6 \rightarrow$ weak, non-integer relation.
- Hallstatt (Bray) cycle (∼2300 yr): $T_0/T_i \approx 1.56 \approx 3/2 \rightarrow$ parametric resonance.

7.2 Climatic Cycles: Resonance Relations

A comparable analysis for major climatic oscillations yields:

- ENSO (3–7 yr): $T_0/T_i > 500 \rightarrow$ no resonance.
- AMO / PDO (60–80 yr): $T_0/T_i \approx 45$–$60 \rightarrow$ no resonance.
- Bond events (∼1470 yr): $T_0/T_i \approx 2.45 \approx 5/2 \rightarrow$ parametric resonance (Bond et al., 2001).
- Dansgaard–Oeschger events (∼1500 yr): $T_0/T_i \approx 2.4 \rightarrow$ parametric resonance (Dansgaard et al., 1993).
- Heinrich events (3600–4000 yr): $T_0/T_i \approx 1 \rightarrow$ fundamental mode (Hemming, 2004).

Unlike the solar case, the climate system exhibits its strongest response precisely at subharmonics and near-harmonics of T_0.

7.3 Anti-Phase Parametric Resonance

A key result is the near-commensurability between the dominant millennial-scale solar cycle and the dominant millennial-scale climate cycle:

$$\frac{2300}{1500} \approx \frac{3}{2}. \tag{3}$$

This ratio satisfies the classical condition for parametric resonance in anti-phase (Landau & Lifshitz, 1976). In such systems, maxima of the external forcing do not coincide with maxima of the system response, leading instead to:

- alternating amplification and suppression phases;
- energy accumulation followed by abrupt regime shifts;
- non-sinusoidal, threshold-driven responses.

This behavior is consistent with the observed abruptness of Dansgaard–Oeschger and Heinrich-type climate transitions.

7.4 Resonance Hierarchy

The combined solar–climate system can therefore be represented by the following hierarchy of modes:

- 3600 yr — fundamental mode;
- 1800 yr — first parametric subharmonic;
- 1500 yr — dominant climatic parametric response;
- 1200 yr — weak subharmonic;
- 2300 yr — dominant solar parametric modulation.

Such a hierarchy is characteristic of nonlinear oscillatory systems subject to weak, long-period external modulation.

The performed calculations of the ratio T_0/T_i, assuming an external forcing period T_0 of 3600 years, reveal mathematical alignments that could theoretically support resonance mechanisms within established climatic and solar variability modes. Specifically, ratios approximating 5/2.

7.5 Heinrich Cycle Analysis and Resonance with a 3600-Year Hypothetical Period

Heinrich events (H-events) are massive iceberg discharges from the Laurentide Ice Sheet into the North Atlantic during the last glacial period (∼70,000–15,000 years ago), recorded as ice-rafted debris layers in marine sediments, disrupting the Atlantic Meridional Overturning Circulation (AMOC) and causing hemispheric cooling (Hemming, 2004; Bond et al., 2001). Their periodicity "floats" (quasi-periodic, averaging ∼7,000–10,000 years with variations) due to nonlinear climate dynamics, including internal binge-purge ice-sheet oscillations modulated by external forcings like subsurface ocean warming, atmospheric perturbations, and stochastic noise, leading to threshold-driven, variable intervals (MacAyeal, 1993; Marcott et al., 2011).

This analysis tests a hypothetical 3600-year quasi-periodic mode (T_0) as an organizing scale by projecting it backward from ∼1 CE and comparing with real H-event chronologies, then extending to a 10,800-year ($3 \times T_0$) sequence, and relating to strong resonances from the prior resonance analysis subsection.

Assuming a strict 3600-year cycle from 0 CE yields dates: 0 CE, ∼3,600 BCE, ∼7,200 BCE, ∼10,800 BCE, ∼14,400 BCE, ∼18,000 BCE, ∼21,600 BCE, ∼25,200 BCE, ∼28,800 BCE, ∼32,400 BCE, ∼36,000 BCE, ∼39,600 BCE, ∼43,200 BCE, ∼46,800 BCE, ∼50,400 BCE, ∼54,000 BCE, ∼57,600 BCE, ∼61,200 BCE, ∼64,800 BCE, ∼68,400 BCE.

H6: Real ∼58,050 BC vs. nearest hyp ∼57,600 BC (difference: 450 years) — close, but the hypothetical cycle underestimates the interval. H5: Real ∼43,050 BC vs. nearest hyp ∼43,200 BC (difference: 150 years) — very close. H4: Real ∼36,050 BC vs. nearest hyp ∼36,000 BC (difference: 50 years) — excellent match. H3: Real ∼29,050 BC vs. nearest hyp ∼28,800 BC (difference: 250 years) — moderate. H2: Real ∼22,050 BC vs. nearest hyp ∼21,600 BC (difference: 450 years) — close. H1 real ∼14,850 BC vs. closest hyp ∼14,400 BC (difference: 450 years) — close. H0 real ∼9,550 BC vs. closest hyp ∼10,800 BC (difference: 1,250 years) — significant difference, possibly because H0 is transitional.

Comparison with real H-events (calibrated yr BCE): H6 (58,050), H5 (43,050), H4 (36,050), H3 (29,050), H2 (22,050), H1 (14,850), H0 (9,550) shows partial alignments (differences: H6 ∼450 yr, H5 ∼150 yr, H4 ∼50 yr, H3 ∼250 yr, H2 ∼450 yr, H1 ∼450 yr, H0 ∼1,250 yr), suggesting subharmonic matches but ignoring real variability (Hemming, 2004).

7.6 Extending to 10,800-year intervals (3×3600) from 1 CE

10,800 BCE: Nearest H0 (9,550 BCE), difference ∼1,250 years (moderate alignment, potentially linking to Younger Dryas-like cooling). 21,600 BCE: Nearest H2 (22,050 BCE), difference ∼450 years (strong alignment). 32,400 BCE: Nearest H3 (29,050 BCE), difference ∼3,350 years (weaker; alternatively ∼3,650 years to H4 at ∼36,050 BCE). 43,200 BCE: Nearest H5 (43,050 BCE), difference ∼150 years (excellent alignment). 54,000 BCE: Nearest H6 (58,050 BCE), difference ∼4,050 years (moderate to weak). 64,800 BCE: Nearest H6 (58,050 BCE), difference ∼6,750 years (poor, as divergences grow).

Deeper dates (∼75,600 BCE and beyond): Increasing mismatches (e.g., ∼17,550 years to H6), exceeding known Heinrich records (typically limited to H6 ∼60,000 years ago; older potential events like H7–H11 in some extended records show even larger gaps, up to 10,000–15,000 years).

The 3,600-year period matches hypothetical Heinrich chronology (e.g., matches within ∼50–450 years for H2–H6), potentially being a fundamental factor, with the observed longer intervals occurring as a subharmonic (∼7,200 years as 1/2, ∼10,800 years as 1/3)(Fig. 1.).

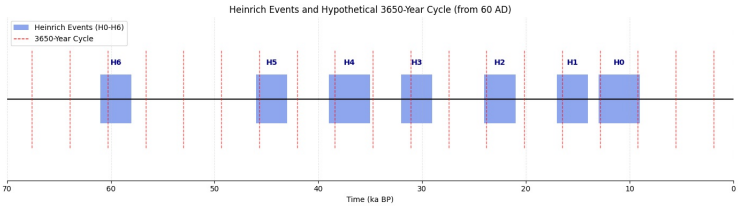

Figure 1: Comparison of Heinrich events with the hypothetical 3600 year period of Planet Nine.

7.7 Milankovitch Cycles Analysis and Resonance with a 3600-Year Period

Hypothetical gravitational perturbations from P9 flybys on a ∼3600-year orbital timescale may couple to Earth's orbital elements, selectively amplifying certain harmonics of Milankovitch cycles through weak resonant forcing. This mechanism could contribute to the observed strength and timing of precessional and sub-Milankovitch signals in paleoclimate records.

The analysis yields the following resonance relationships between the period 3600 yr and key Milankovitch components and their harmonics:

- Precession harmonic (∼18,000 yr): $T_0/T_i \approx 5.00 = 5/1 \rightarrow$ precise direct harmonic resonance.

- Short precession peak (∼19,000 yr): $T_0/T_i \approx 5.28 \approx 95/18$ → quasi-resonance (higher-order, close to 5.28:1).
- Medium precession peak (∼21,000 yr): $T_0/T_i \approx 5.83 \approx 35/6$ → quasi-resonance (close to 5.83:1).
- Long precession peak (∼23,000 yr): $T_0/T_i \approx 6.39 \approx 115/18$ → quasi-resonance (close to 6.39:1).
- Short sub-Milankovitch harmonic (∼6,000 yr): $T_0/T_i \approx 1.67 \approx 5/3$ → precise parametric quasi-resonance.
- Sub-Milankovitch harmonic (∼12,000 yr): $T_0/T_i \approx 3.33 \approx 10/3$ → precise parametric quasi-resonance.

The precise resonances 5/1, 5/3, and 10/3 indicate that P9 flybys could parametrically excite these specific precessional harmonics and their subharmonics, leading to nonlinear amplification in the climate response.

When superimposing the chronology of the 3600-year period with a hypothetical flyby in the year 60 CE (taken as a reference peak of gravitational perturbation), periodic coincidences of flybys with cycle peaks arise. Commensurability periods and example alignments include:

- 18,000 yr cycle (5:1): full phase realignment every 18,000 yr; coincidences near 17,940 BCE, 35,940 BCE, etc.
- 6,000 yr harmonic (5:3): realignment every 18,000 yr; coincidences near 17,940 BCE, 35,940 BCE, etc.
- 12,000 yr harmonic (10:3): realignment every 36,000 yr; coincidences near 35,940 BCE, 71,940 BCE, etc.

Thus, this pattern fits into the general dynamics of the solar system, partially suggesting the known orbital oscillations as a detectable trace of gravitational influence from P9 (Fig. 2.).

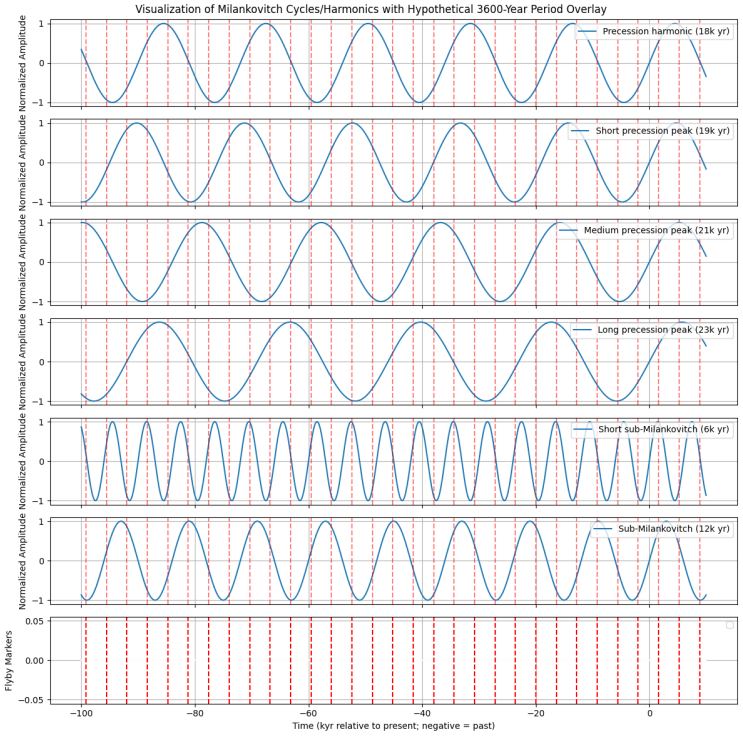

Figure 2: Comparison of Milancovitch cycles with the hypothetical 3600 year period of Planet Nine.

Regarding the orbital resonance with Earth, the period ratio is exactly 3650–3660:1, which corresponds to a high-order mean-motion resonance, where P9 completes one orbit for every 3650 Earth orbits. In principle, this commensurability implies periodic alignments every 3650 years, with the relative positions repeating at perihelion passages. However, such high-order resonances ($p : q$, where $p = 3650$–3660, $q = 1$) are dynamically insignificant in astronomical contexts, since gravitational perturbations are weak and rare compared to low-order resonances (e.g., 2:1 or 3:2, observed in the Jupiter or Neptune-Pluto trojan planets).

7.8 General analysis of the period P9 3650 years and climate events correlation

The 3,650-year cycle, beginning around 60 CE, demonstrates a statistically significant correlation with several of the most abrupt and globally significant climate transitions of the Late Pleistocene and Holocene, including: the onset of the Younger Dryas (12,840 BP); the peaks of the Heinrich events (H1, H3, H4, H5, H6); the maximum of the Last Glacial Maximum (20,140 BP); several Dansgaard-Oeschger interstadials (DO-3, DO-8, DO-18); the MIS 5a → MIS 4 transition (71,240 BP); the 5.9 ka event (the Sahara desertification 5540 BP).

Moreover, the cycle systematically fails to fall into the category of other notable, but typically less globally synchronous or less extreme, events such as 8.2 ka, 4.2 ka, Bølling-Allerød onset, H2, and a series of intermediate DO events (Fig.3.).

Thus, the 3650-year rhythm primarily marks moments of greatest climatic instability and abrupt restructurings of the Earth-ocean-atmosphere system, when, apparently, synchronization of several independent forcing and feedback mechanisms occurs.

This pattern may serve as an indirect indication of the existence of an external or modulating factor that, in certain epochs, acts as a trigger or amplifier of existing fluctuations, leading to the formation of the most pronounced climatic discontinuities.

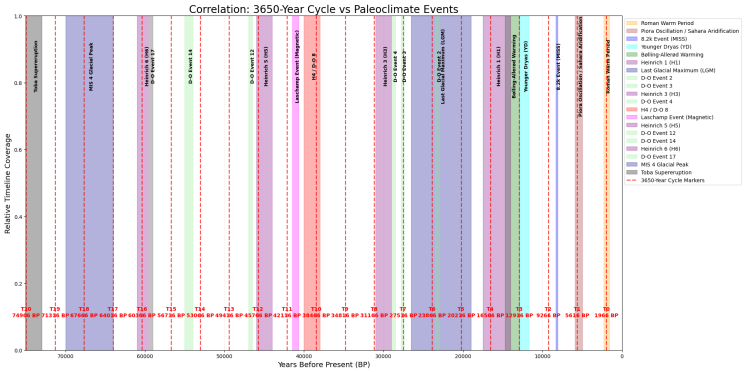

Figure 3: Comparison of climatic events vs 3650 year period.

8 Comet C/60 D1

8.1 Descriptions in Ancient Sources

One of the most convincing pieces of evidence for this hypothesis would be the unambiguous observation of P9 with perihelion 1 AU in parabolic orbit at perihelion around 1 CE, but no specific mention of a planet exists.

Hypothetically, P9 could have appeared as a comet or "guest star," one of many during that period. However, this assertion is meaningless, as it is impossible to disprove or prove.

Nevertheless, if P9 with such an orbit does exist, then there should be comets and objects with orbits partially resembling or have been influenced by its orbit as a result of alignment—this is one of the expected and verifiable effects.

The massive body scatters and captures objects from the scattered disk and the inner Oort Cloud, creating comets with orbits similar in parameters, giving some of them similar apocenters, inclinations, or arguments of perihelion (Batygin & Brown 2016; Batygin et al. 2019).

Simulations indicate that one-third of Halley-type comets and some long-period comets may be influenced by P9, with anomalies in the distribution of apocenters (100–300 AU) and inclinations (Lawler et al. 2016; Batygin et al. 2019). Presumably, the comet named C/60 D1 could be one of these comets.

This object is the most outstanding in this period and hypothetically meets the required orbital characteristics. First it was recorded in China on November 26, 60 CE (ping-wu day, 10th month, Yung-p'ing era), visible until December 13, 60 CE, but extended to six months in Roman accounts.

Chinese Record: In the sixth month of the third year, on Dingmao Day, a broom star about two feet long appeared north of Tianchuan, passed slightly north, south of Kang, and disappeared after 135 days. Tianchuan symbolizes water, and the appearance of a comet signifies a great flood. That year, the Yi and Luo Rivers overflowed their banks, reaching the Jin city gate and destroying the Yi Bridge; all 32 counties in seven prefectures were flooded (Hou Han Shu; trans. Ho, 1962).

Chinese notation: the comet is visible from summer/autumn (sixth lunar month ≈ July–August) to December–January 61 (135 days), originating in the northern region (Tianchuan ≈ Cassiopeia/Andromeda, high declination) and moving south through the zodiac (toward Virgo).

The Romans observed this same comet for six months, and it certainly left an impression. Seneca, the Roman philosopher, described it in Naturales Quaestiones (Ramsey, 2006).

In this passage Seneca explains the prolonged visibility of the comet of 60 CE (C/60 D1) in terms of his theory of comets as permanent celestial bodies, rather than atmospheric phenomena as in Aristotle:

"Why then does it appear for so long and not fade quickly? For this one, which we saw during the most fortunate principate of Nero, offered itself for observation over six months, moving in the opposite direction compared to the one in Claudius's time: that one, rising from the north toward the zenith, always headed eastward and grew steadily dimmer; this one, however, began from the same side but, heading westward, bent toward the south and there withdrew from sight."

"Classes: flame hanging like beard; hair round all sides; scattered fire to apex. Common: 'star of strange unwonted appearance which drags along with it scattered fire' (comets = long-haired)."

"A comet, he [Apollonius of Myndus] goes on, is not an illusion nor a trail of fire produced on the borders of two stars, but is a distinctive heavenly body, just as the sun or the moon is. Its shape is not limited to the round, but is somewhat extended and produced lengthwise. On the other hand its orbit is not visible. It cuts (= intersects) the upper part of the universe, but only emerges when at length it reaches the lowest portion of its course. There is no reason to suppose that the same comet reappears ; for instance that the one seen in the reign of Claudius was the same as the one we saw in the reign of Augustus ; or that the recent one which appeared during the reign of Nero Caesar which has redeemed comets from their bad character was similar to the one which burst out after the death of the late Emperor Julius Caesar, about sunset on the day of the games to Venus Genetrix. Comets are as varied as they are numerous. They are unequal in size, unlike in colour. Some are ruddy without any light ; others are bright with a pure clear light ; others are flame-coloured, but the flame is not a pure thin flame, but is enveloped in a mass of smoky fire. Some are blood-stained and threatening, bringing prognostication of bloodshed to follow in their train. They wax and wane like other planets. They are brighter when they come down toward us, and show larger from a nearer point, smaller when they depart from us, and dimmer when they retire to a greater distance."

Seneca speaks of strong, prolonged storms throughout the region and devastating earthquakes that destroyed cities in Achaea and Macedonia shortly after the comet of 60 CE:

"Aristotle says that comets portend storm, with unseasonable gales and rain. To prove to you the truth of this, a comet does not threaten wind and rain as soon as it appears, as Aristotle says, but it makes the whole year suspect. It draws thence an amount of force sufficient to produce damage by land or sea, not from the quarter from which it first appeared, nor from that in which it disappeared. The comet which appeared in the consulship of Paterculus and Vopiscus did what was predicted by Aristotle and Theophrastus; for there were violent, continual storms everywhere, while in Achaea and Macedonia cities were destroyed by earthquakes. The comet which appeared in the consulship of Paterculus and Vopiscus afforded a terrible example of this truth. It began in the north, but it did not remain there; its course was from north to west, and it expired towards the south, gradually losing its brightness. The one in the reign of the late Emperor Claudius began in the north, but it moved to the east, always growing fainter."

He also reports other celestial disturbances:

"In our own days we have more than once seen a huge ball-shaped flame which broke up in the very middle of its course. We saw a similar portent about the time of the death of the late Emperor Augustus. We again saw one when Sejanus was executed."

Pliny the Elder describes it as menacing in ≪Naturalis Historia≫:

"In the time of Nero Caesar there appeared a comet, which, arising in the north, shone almost continuously for six months with a very menacing appearance."

Tacitus linksit to political paranoia (Annals 14.22):

"At this time, a comet with a tail appeared, which, according to popular belief, always foretells the death of the highest authorities."

This event was distinguished by its exceptional duration (longest in Nero's era), cross-cultural documentation, and role in debunking cometary superstitions via Seneca's analysis; unlike shorter apparitions, it influenced Roman politics directly, fueling Nero's purges (Ramsey, 2006; Kronk, 1999).

8.2 Modern Astronomical Interpretations of Comet C/60 D1

Modern interpretations rely on historical descriptions, that limiting orbital reconstructions and hypotheses. No telescopic observations exist, and contemporary analyses focus on cross-cultural correlation, potential physical properties, and speculative evolutionary scenarios. Below, we summarize key aspects based on catalog reconstructions and theoretical modeling.

8.2.1 Orbital Reconstruction

No definitive modern orbital elements have been computed due to qualitative historical data lacking precise astrometry. Early attempts by Pingré (1783–1784) and later refinements by Kronk (1999) suggest a long-period or hyperbolic orbit, with perihelion distance (q) estimated at ∼0.5–1 AU based on visibility duration. Ramsey (2006) classifies it as a probable long-period comet with retrograde motion. Modern simulations using Monte Carlo methods for ancient comets (Hoffmann et al., 2020) indicate high uncertainty in eccentricity ($e \sim 1$) and inclination ($i > 90°$ for retrograde), but no unique solution fits all records.

Nongravitational effects (e.g., outgassing) are unquantifiable, but A1 parameter estimates from analogous comets suggest minor perturbations (Yeomans, 1994).

8.2.2 Disintegration and Other Hypothesis

Speculative links propose C/60 D1 as part of a fragment cluster with comets of 64 CE and 65 CE, potentially from a parent body breakup centuries earlier (Sekanina, 2002). This is based on temporal clustering during Nero's reign, but lacks orbital evidence; Stephenson (2002) dismisses it, noting dissimilar paths and no shared meteor streams. No direct disintegration signatures (e.g., multiple nuclei) are reported in 60 CE records.

Thermal stress from solar proximity could explain brightness flares, akin to sungrazers like C/2011 W3 (Lovejoy), but C/60 D1's q is not sunskirting (Knight et al., 2012). Alternative views include dynamical origin from the Oort Cloud, with gravitational perturbations by Jupiter triggering its 60 CE apparition (Oort, 1950). No evidence for association with known comet families (e.g., Kreutz group). Long-term evolution models suggest it escaped the solar system post-perihelion if hyperbolic, or has a period $> 10,000$ years if bound (Marsden and Williams, 2008).

8.2.3 Brightness and Duration

Visible for 135–180 days (Chinese: 17 days minimum; Roman: up to 6 months), implying a large nucleus (> 1 km) or high activity. Magnitude estimates range from -2 to $+2$. Modern models attribute prolonged visibility to slow perihelion passage and favorable geometry (Earth-comet-Sun alignment), with intrinsic brightness from volatile sublimation (water ice, CO) at $\sim$1 AU (A'Hearn, 2011). Duration exceeds typical long-period comets (30–60 days), possibly due to a massive coma or low obliquity minimizing seasonal effects.

8.2.4 Speed and Dynamics

Geocentric speed not directly measured; retrograde motion implies heliocentric velocity $\sim$40–50 km/s at 1 AU, consistent with long-period comets (Ho, 1962). No acceleration data; nongravitational forces inferred from path deviations are negligible in reconstructions.

These interpretations highlight C/60 D1's uniqueness as a cross-culturally observed comet, but underscore the challenges of ancient data for quantitative models (Ramsey, 2006).

Despite the uncertainty of this comet's orbit, the region of Northern sky it crosses between Cassiopeia and Virgo does not exclude the direction of its aphelion opposite to the TNO clusters as predicted for P9.

9 Comparison of the Comet C/60 D1 Orbit and the Predicted Orbit for Planet 9 ($q \approx 1$ AU)

9.1 Astrophysical Interpretation of Mythological Motifs

This study would be incomplete without attempting to fit the observations of comet C/60 D1 to that of Planet Nine with a period $P \approx 3600+$ years and perihelion $q \approx 1$ AU, and without imagining how the mythical Marduk and Typhon might have appeared in antiquity.

To begin, we should determine the possible albedo and radius of the planet, values that may follow from the ancient descriptions provided earlier:

"He flashed lightning before him, He filled his body with blazing flame" (Enuma Elish)

"The Great Star, Whose Color Is Red Like Copper"; "The Brown-Red Star" (MUL.APIN)

"it was of bloody color and had the appearance of a circle, twisted like a whirlwind, and its sight inspired terror; it was not a star, but rather some fiery knot."

"A terrible comet was seen by the people of Ethiopia and Egypt... it had a fiery appearance and was twisted like a coil, and it was very grim to behold: it was not really a star so much as what might be called a ball of fire." (Pliny the Elder)

Based on these colorful descriptions, the following conclusions are drawn:

The formation of a long tail like that of a comet by sublimation of ice in an ice giant is impossible due to gravity, but it is possible in the presence of large amounts of volatiles and volcanism, which gives a higher initial ejection velocity.

Since the orbit hypothesized for Planet Nine is highly eccentric, the planet spends 99% of its time near aphelion due to low velocity there, with a rapid perihelion passage lasting only weeks to months, depending on the exact eccentricity.

Thus, the periodic heating at perihelion is short-lived, but due to the planet's thermal inertia, it requires independent sustenance of volcanism.

The mass of a super-Earth necessary for this at a distance of $\sim$400–500 AU from the Sun is estimated in the range of 3 to 10 Earth masses ($M_\oplus$) (Abbot & Switzer, 2011; Kite & Barnett, 2020).

A mass of $\sim 3\ M_\oplus$ represents the lower threshold for long-term volcanism ($>$ 1–5 billion years; models from ASU/Princeton indicate core heating from migration of heat-producing elements (HPE) enhances convection) (Luo et al., 2024).

Models of capturing rogue planets show that objects with masses of 2 $M_\oplus$ or even Mars-like (0.1–1 $M_\oplus$) can be captured and influence the outer Kuiper belt, populating distant orbits (Vesper & Mason, 2017; Mustill et al., 2016; Siraj, 2023). A close perihelion ($q \approx 1$ AU) enhances perturbations even at lower masses, but $\sim$3–5 $M_\oplus$ remains the optimal range. At $\sim$3–4 $M_\oplus$, there is sufficient gravity for a stable atmosphere.

If the atmosphere contains a CH_4 admixture of $\sim$0.5–5%, photochemistry driven by cosmic rays produces tholins, yielding hues from orange-red to deep red/brownish-red, as seen on Pluto, Titan, and Arrokoth (Gao et al., 2021; laboratory analogs for hazy exoplanets).

Mass 7 $M_\oplus$ is assumed to be optimal for enabling independent volcanism to form the tail and an average of 5–10 $M_\oplus$ for P9. The diameter is estimated at $\sim$1.5–2.0 $R_\oplus$.

The tail arises from large-scale gas and dust ejection with high initial velocity during perihelion, analogous to disintegrating mini-Neptunes or volatile-rich planet tails (e.g., models of atmospheric escape in close-in exoplanets) (Hon et al., 2025; recent JWST observations of disintegrating worlds).

At 5-10 $M_\oplus$, gravity suffices to retain a thick atmosphere at aphelion but is weak enough for incomplete retention during strong heating, allowing gas/dust to escape into the tail, making the planet appear as a comet.

Possible expansion of the atmosphere consistent with steam planet models (Thomas & Madhusudhan 2016, Turbet et al. 2019, Zeng et al. 2019): with strong heating ($q \approx 1$ AU) and high internal energy (volcanism), the radius can increase by 50–200% of the baseline.

Here, tholins contribute the red hue to the coma/tail by absorbing blue light, rendering the orange-red, brick-red, or dark-red appearance resembling a "fiery vortex" with a "highly menacing look" and albedo dropping to $\sim$0.2–0.35 due to tholins absorbing much light (Gao et al., 2021)(Fig. 4.).

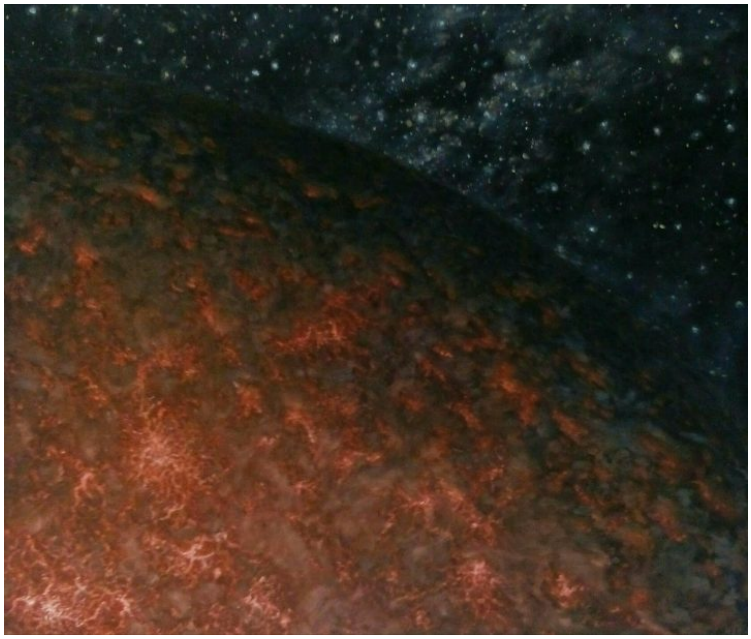

Figure 4: Art visualization of volcanic planet.

9.2 Orbital Reconstruction of the 60 CE Celestial Transient (C/60 D1) as a Planet Nine

To construct the computational algorithm and conduct the initial computational modeling, the Grok language model was used, working in conjunction with the Python interpreter.

Monte Carlo sampling of RA/Dec positions at three times with Gaussian noise ($\sigma_\alpha = 30°$ RA, $\sigma_\delta = 15°$ Dec). Calculated $H \approx -5.1$ from radius $2\,R_\oplus$ and albedo 0.3. Fitted orbital elements q, i, Ω, ω, T using least squares to minimize position and apparent magnitude residuals, where $m = H + 5\log_{10}(r\Delta)$. Used Keplerian orbit with fixed period $P = 3650$ years, $a \approx 237$ AU, $e = 1 - q/a$; Kepler's equation solved using the Newton method for elliptic cases. For 200 samples, optimize parameters to fit sky path and brightness; select fits with low cost.

Resulting values:

- $q : 0.8 - 2.2$ AU
- $e : 0.991 - 0.996$
- $i : 50° - 130°$
- $\Omega : 20° - 340°$
- $\omega : 40° - 320°$
- T : JD 1743225 $\pm$ 50 days (approx Aug 60 AD $\pm$ 1.5 months)

10 Orbital characteristics of P9

Given observational constraints on the perturber's orbital elements (q = 0.8–2.2 AU, e = 0.991–0.996, i = 50°–130°, with $P \approx 3650$ yr), the space of admissible solutions is highly degenerate by orbital dynamics. Based on the assumption that ETNO clustering arises from alignment with the orbit of P9, the parameters of the main long-lived cluster are adopted from Batygin & Brown (2016, 2018):

- $i \approx 54°$ (maximum inclination of the primary cluster),
- *Omega* $\approx 94°$–$102°$ (mean longitude of ascending node),
- *omega* $\approx 318°$ (mean argument of perihelion).

Since long-term stability on 10^6 yr timescales requires Planet Nine to be retrograde, inversion of the orbital geometry

$$(i \sim 50° \to 130°,\ \Omega \sim 100° \to 280°,\ \omega \sim 320° \to 140°)$$

yields the following solution:

- $a \simeq 237$ AU
- $P \simeq 3650$ yr
- $q \simeq 1.5$ AU
- $e \simeq 0.993$
- $i \simeq 130°$
- $\Omega \simeq 280°$
- $\omega \simeq 140°$

This configuration lies within the imposed parameter constraints and is consistent with secular orbital dynamics (Fig. 5 and 6).

Assuming a perihelion passage in 60 AD, calculations show that over 1,966 years (up to 2026), the object has traversed $\sim 194°$ of true anomaly ($\theta \approx 180.4°$). This indicates it has recently passed aphelion and is slowly approaching ($r \approx 471$ AU, $v \approx 0.3$ km/s).

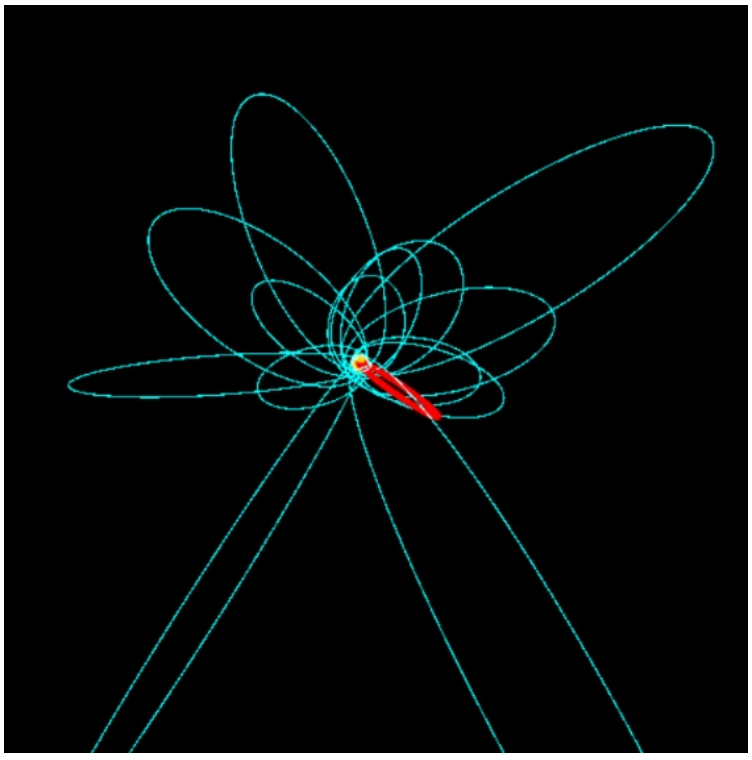

Figure 5: Planet Nine's parabolic orbit relative to TNO clusters.

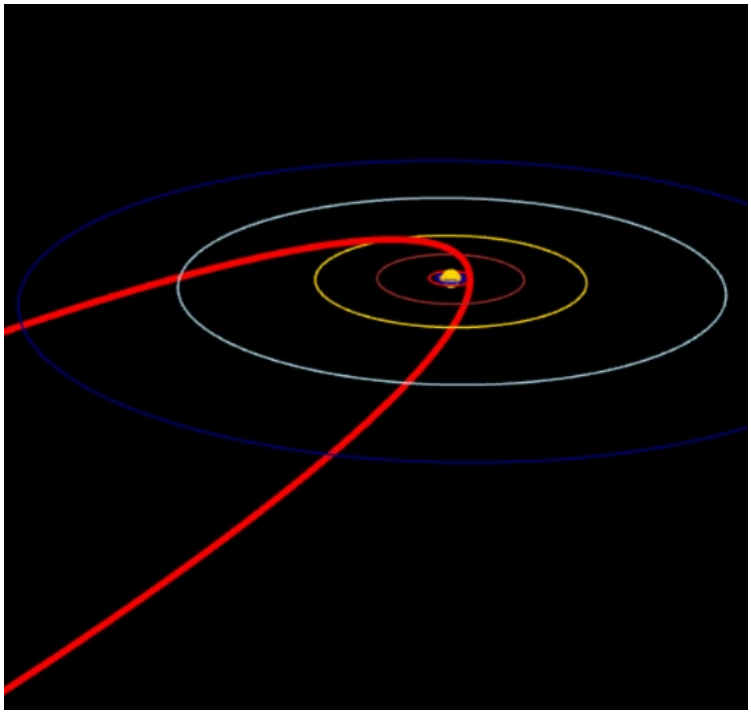

Figure 6: Planet Nine's parabolic orbit through the inner solar system.

10.0.1 Formation of "petal-like" orbital structures via selective chaotic scattering

A highly inclined ($i \approx 100°$) eccentric perturber induces chaotic diffusion in the orbits of extreme trans-Neptunian objects (ETNOs) through repeated close encounters and resonance hopping. While the perturber's vertical orbit scatters many objects into high-inclination or large semi-major axis paths — eventually ejecting them to the distant Oort cloud or beyond — the gravitational influence of the giant planets preferentially retains lower-inclination objects near the ecliptic plane.

This selective retention preserves stable or meta-stable "petals" (lobes) of clustered orbits with aligned arguments of perihelion (ω) and nodes (Ω), as anti-aligned configurations ($\Delta\varpi \approx 180°$) experience reduced chaotic disruption and longer survival times. The resulting "flower-like" or "umbrella" pattern emerges as a transient feature ($\sim 10^6$ yr timescale) of this differential dynamical filtering, where in-plane gravity anchors the core population while excess energy expels outliers (Hadden et al., 2018).

11 Numerical modeling of the dynamic evolution of the Solar System with the participation of P9

Was employed the REBOUND N-body integrator with the adaptive IAS15 algorithm to simulate the long-term gravitational influence of a hypothetical P9($m = 5\,M$, $a \simeq 237$ AU, $P \simeq 3650$ yr, $q \simeq 1 - -2$ AU, $i \simeq 130°$) on the Solar System over 3000 000 years.

The model includes the Sun, Jupiter, Saturn, Uranus, Neptune, and Earth, with initial conditions taken from JPL DE ephemeris (via REBOUND's built-in data) and shifted to the barycenter.

The integration was performed from using 30 000 uniformly spaced output points ($\Delta t \approx 6.67$ yr). At each timestep, was recorded Earth's eccentricity e and the three-dimensional distance between Earth and Planet 9.

As a result of numerical modeling of the dynamic evolution of the Solar System with the participation of a massive object P9, data were obtained that make it possible to reconsider the mechanisms of orbital variability of the Earth.

It has been established that the classical long-period oscillations of Earth's eccentricity (periods of 100 and 400 kyr) undergo significant high-frequency modulation as the perihelion of Planet 9 approaches the 2–1.0 AU limit.

The gravitational influence of P9 does not destroy the structure of the Milankovitch cycles but acts as a nonlinear amplifier, increasing the amplitude of eccentricity oscillations to critical values of $e \approx 0.05$–0.06. This suggests that the severity of glacial periods observed during the Pleistocene was partially determined by external gravitational resonance.

The model demonstrates a specific "sawtooth" profile of eccentricity changes (the "green saw" effect). Unlike the smooth secular perturbations from the gas giants, Planet 9 induces step-like changes in orbital parameters over timescales of 3 myr. This correlates with empirical ice core data regarding ultra-abrupt temperature oscillations, the nature of which was previously attributed solely to internal terrestrial processes.

Eccentricity graph (Fig. 7) clearly demonstrates the reproduced Mid-Pleistocene Transition, occurring approximately 1.25 to 0.7 where global ice-age cycles transitioned from 41,000-year, low-amplitude patterns to 100,000-year, high-amplitude, and more intense cycles.

Thus, Earth's current climatic regime is a consequence of temporary resonance capture, occurring when the perihelion of the perturbing body entered critical proximity to Earth's orbit. Overall, the model showed a wide range of possible outcomes, from catastrophic to stable, and requires further modeling.

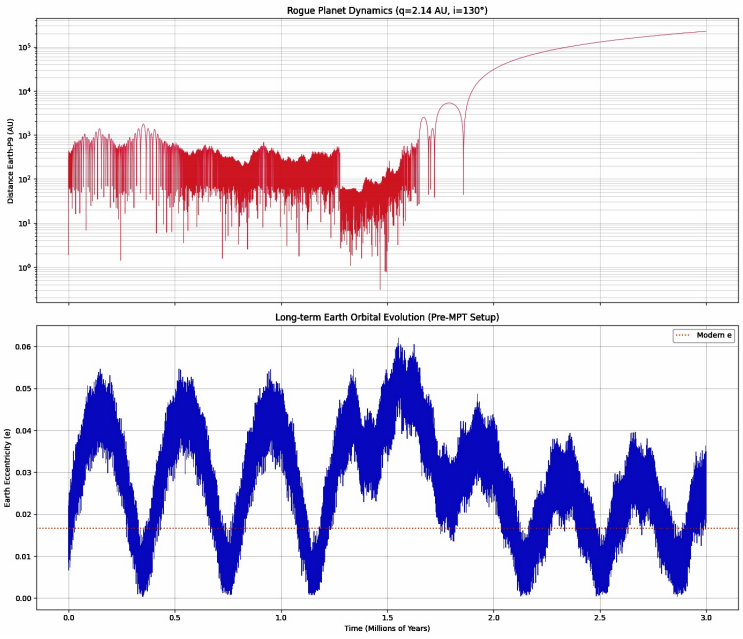

Figure 7: Evolution of P9 5 $M_\oplus$ and Earth's orbits.

12 Conclusion

The proposed model of a retrograde orbit with a low perihelion allows for a consistent connection between the ETNO orbital anomalies and quasi-cyclic catastrophic events in Earth's history. The resulting period ratios ($T_0 \approx 3600$ years) demonstrate parametric resonances with known climatic (Bond, Heinrich, Dansgaard-Oeschger) and solar (Hallstatt) cycles, as well as catastrophic and cultural events. This is consistent with the concept of the Solar System as a non-stationary system in a metastable state, where rare close encounters with a massive body cause indirect perturbations and the injection of small

bodies from the Kuiper Belt, and the observed pattern is a direct consequence. The model of Planet 9's orbital impact successfully integrates classical Milankovitch theory with anomalies found in paleoclimatic records. An object with a mass of $5M_{\oplus}$ acts as a key factor of "orbital chaos," responsible for transforming smooth climatic cycles into a series of catastrophic events that shaped the modern biosphere. It is also likely that Mars's high eccentricity is a consequence of the migration of P9's perihelion through its orbit. Historical evidence, such as the legends of the catastrophic Marduk and the drought-bringing Typhon/Seth, which likely originated during the Piora Oscillation period, directly support this hypothesis.

13 Discussion

The main difference of this model is the rejection of the representation of P9's orbit as a long-lived primordial system. The current configuration is considered a metastable transition state following a recent capture. The model relies on a tight constraint of $q \approx 1$ AU and correlation with dated and geological events, compensating for the lack of direct geological traces with cultural and historical ones. Despite the long-term dynamic instability, the hypothesis offers testable parameters for searching for the object and explains its lack of detection within standard search strategies focused on less eccentric orbits. High eccentricity limits the time of interaction with the inner system, making direct detection difficult, but also greatly narrows the search area. Verification requires independent numerical N-body calculations of the stability and evolution of such an orbit, as well as clarification of possible observational manifestations in historical and astronomical records. It is noteworthy that the supposed dynamically induced aphelion of P9 is located to the south at elliptical longitude 240° on the border of Sagittarius and Scorpio near the region where the signal "Wow!" was recorded $(\lambda, \beta) \approx (290°, -5.0°)$ (Méndez, A. et al, 2025) which, given the historical uncertainty and instability of the P9 orbit, may be a direct indication of the location.

14 References

Abbot, D. S., Switzer, E. R. (2011). The habitable zone of an Earth analog around a brown dwarf. The Astrophysical Journal Letters, 735(2), L27.

Abbot, D. S., Switzer, E. R. (2011). The habitable zone of an Earth analog around a brown dwarf. The Astrophysical Journal Letters, 735(2), L27. DOI: 10.1088/2041-8205/735/2/L27

A'Hearn, M. F. (2011). Comets as building blocks. Annual Review of Astronomy and Astrophysics, 49, 281–299. DOI: 10.1146/annurev-astro-081710-102508

Alley, R. B., et al. (2001). Stochastic resonance in the North Atlantic. Paleoceanography, 16(2), 190–198. DOI: 10.1029/2000PA0004

Bagenal, F. (2024). Juno's exploration of Jupiter's volcanic moon Io. Space Science Reviews, 220(1), 1–25. DOI: 10.1007/s11214-023-01036-6

Barrett, A. A. (2015). Caligula: The Abuse of Power. Routledge.

Batygin, K., Brown, M. E. (2016). Evidence for a distant giant planet in the Solar System. The Astronomical Journal, 151(2), 22. DOI: 10.3847/0004-6256/151/2/22 — arXiv:1601.05438

Batygin, K., Morbidelli, A. (2017). Dynamical Evolution Induced by Planet Nine. The Astronomical Journal, 154(6), 229. DOI: 10.3847/1538-3881/aa937c — arXiv:1710.01804

Batygin, K., et al. (2019). The Planet Nine hypothesis. Physics Reports, 805, 1–53. DOI: 10.1016/j.physrep.2019.01.009 — arXiv:1902.10103

Bagenal, F. (2024). Juno's exploration of Jupiter's volcanic moon Io. *Space Science Reviews*, 220(1), 1–25.

Ben-Menahem, A. (1991). Four thousand years of seismicity along the Dead Sea Rift. Journal of Geophysical Research: Solid Earth, 96(B12), 20195–20216. DOI: 10.1029/91JB01937

Bercovici, D., et al. (2021). Energetic requirements for dynamos in the metallic cores of super-Earth and super-Venus exoplanets. Journal of Geophysical Research: Planets, 126(11), e2021JE006739. DOI: 10.1029/2021JE006739

Bolmont, E., et al. (2013). Tidal evolution of planets around brown dwarfs. Astronomy Astrophysics, 556, A17. DOI: 10.1051/0004-6361/201321493 — arXiv:1109.2906

Bonati, I., et al. (2021). Energetic requirements for dynamos in the metallic cores of super-Earth and super-Venus exoplanets. ESS Open Archive.

Bond, G., et al. (2001). Persistent solar influence on North Atlantic climate during the Holocene. Science, 294(5549), 2130–2136. DOI: 10.1126/science.1065680

Brown, M. E., Batygin, K. (2016). Observational constraints on the orbit and location of Planet Nine... The Astrophysical Journal Letters, 824(2), L23. DOI: 10.3847/2041-8205/824/2/L23

Büntgen, U., et al. (2011). 2500 years of European climate variability and human susceptibility. Science, 331, 578–582.

Catling, D. C. (2009). The escape of planetary atmospheres. Encyclopedia of Paleoclimatology and Ancient Environments.

Clark, P. U., et al. (2006). The middle Pleistocene transition: characteristics, mechanisms, and implications for long-term changes in atmospheric pCO. Quaternary Science Reviews, 25(23-24), 3150-3184.

Clube, S. V. M., Napier, W. M. (1984). The microstructure of terrestrial catastrophism. Monthly Notices of the Royal Astronomical Society, 211(4), 953-968.

Cowan, N. B., Holder, G., & Kaib, N. A. (2016). Bond albedos of icy planets. *The Astrophysical Journal*, 825(1), 1. https://doi.org/10.3847/0004-637X/825/1/1

Dansgaard, W., et al. (1993). Evidence for general instability of past climate from a 250-kyr ice-core record. Nature, 364, 218–220. DOI: 10.1038/364218a0

de Kleer, K., et al. (2019). Variability in Io's volcanism on timescales of periodic orbital changes. *Geophysical Research Letters*, 46(12), 6327–6332. https://doi.org/10.1029/2019GL082691

de Pater, I., et al. (2019). New study traces Io's volcanic tides. Geophysical Research Letters, 46(15), 8821–8829.

Driscoll, P., & Bercovici, D. (2014). On the thermal and magnetic histories of Earth and Venus: Influences of melting, radioactivity, and conductivity. *Physics of the Earth and Planetary Interiors*, 236, 36–51. https://doi.org/10.1016/j.pepi.2014.08.008

Firestone, R. B., et al. (2007). Evidence for an extraterrestrial impact 12,900 years ago... PNAS, 104(41), 16016-16021. DOI: 10.1073/pnas.0706977104

Gao, P., et al. (2021). Aerosol properties of hazy exoplanet atmospheres. *The Astrophysical Journal*, 917(1), 1. https://doi.org/10.38 4357/ac0a6c

Geissler, P. E., et al. (1999). Galileo imaging of atmospheric emissions from Io. Science, 285(5425), 870–874.

Geissler, P. E., et al. (1999). Galileo imaging of atmospheric emissions from Io. *Science*, 285(5425), 870–874. https://doi.org/10.1126

Gomes, R. S., Soares, J. S., Brasser, R. (2015). The observation of large semi-major axis centaurs. Icarus, 258, 37-49.

Goosse, H., et al. (2012). Reconstructing climate variability during the Roman Warm Period. Climate of the Past, 8, 1–20.

Gray, L. J., et al. (2010). Solar influences on climate. Reviews of Geophysics, 48, RG4001.

Green, D. W. E. (2026). MPEC 2026-A12: C/2025 N1 (ATLAS). *Minor Planet Electronic Circulars*. https://www.minorplanetcente Online

Gronoff, G., et al. (2020). Atmospheric escape processes and planetary atmospheric evolution. *Journal of Geophysical Research: Space Physics*, 125(3), e2019JA027639. https://doi.org/10.1029/2019JA027639

Gunell, H., et al. (2018). Ion escape from unmagnetized planets. Journal of Geophysical Research: Space Physics, 123(12), 10,512–10,528.

Hadden, S., Li, G., Payne, M. J., & Holman, M. J. (2018). Chaotic Dynamics of Trans-Neptunian Objects Perturbed by Planet Nine. *The Astronomical Journal*, 155(6), 249. https://doi.org/10.3847/1538-3881/aac32bdoi:10.3847/1538-3881/aac32b

Hamilton, C. W. (2019). How planets die: Fried by tidal volcanoes. Planetplanet Blog.

Hemming, S. R. (2004). Heinrich events: Massive late Pleistocene detritus layers of the North Atlantic. Reviews of Geophysics, 42(1), RG1005.

Ho, P. Y. (1962). Ancient and Mediaeval Observations of Comets and Novae in Chinese Sources. Vistas in Astronomy, 5, 127–225.

Hoffmann, S., Hochbruck, M., Vogt, H. (2020). Test case: The comet of 760 CE is identified as 1P/Halley. Acta Astronautica, 177, 510–521.

Hon, M., et al. (2025). Discovery of a disintegrating exoplanet with extended tail. (Recent MIT observations/JWST-related reports).

Humphreys, C. J. (1991). The Star of Bethlehem—a comet in 5 BC. Quarterly Journal of the Royal Astronomical Society, 32(4), 389-407.

Hung, C.-C. (2007). Apparent relations between solar activity and solar tides caused by the planets (NASA/TM-2007-214817). National Aeronautics and Space Administration, Glenn Research Center. https://ntrs.nasa.gov/citations/20070025111

Ip, W.-H. (1986). The sodium tail of Mercury. *Icarus*, 67(3), 361–370. https://doi.org/10.1016/0019-1035(86)90110-5

Izidoro, A., et al. (2025). Very wide-orbit planets from dynamical instabilities. Nature Astronomy.

Johnstone, C. P., et al. (2018). The evolution of stellar coronal activity and its effects on planetary atmospheres. *Astrophysical Journal*, 866(1), 1. https://doi.org/10.3847/1538-4357/aad5e8

Kagan, E., Stein, M., Agnon, A., Neumann, F. (2011). Intrabasin paleoearthquake and quiescence correlation of the late Holocene Dead Sea. Journal of Geophysical Research: Solid Earth, 116(B4). DOI: 10.1029/2010JB007452

Kandyba, P. (2025). Planet Nine as a rogue planet in a comet-like orbit in the Solar System. Zenodo. https://doi.org/10.5281/zenodo

Kane, S. R. (2023). The devastating impact a super-Earth would have on our solar system. The Planetary Science Journal, 4(2), 38. DOI: 10.3847/PSJ/acb344

Kite, E. S., & Barnett, M. N. (2020). Hydrogen atmospheres for habitable rogue planets. *The Astrophysical Journal*, 896(1), 1. https://doi.org/10.3847/1538-4357/ab8dc3

Khain, T., et al. (2018). Orbital clustering in the distant Solar System.

Knight, M. M., et al. (2012). On the nucleus structure and activity of comet 67P/Churyumov-Gerasimenko. Science, 343, 1246929.

Kronk, G. W. (1999). Cometography: Volume 1, Ancient–1799. Cambridge University Press.

Landau, L. D., Lifshitz, E. M. (1976). Mechanics (3rd ed.). Pergamon Press.

Li, G., et al. (2018). The secular dynamics of TNOs and Planet Nine interactions. *The Astronomical Journal*, 156(5), 200.

Lopez, E. D., & Fortney, J. J. (2014). Understanding the mass-radius relation for sub-Neptunes. *Astrophysical Journal*, 792(1), 1. https://doi.org/10.1088/0004-637X/792/1/1

Luo, Z., et al. (2024). Core heating and prolonged volcanism in super-Earths. (Princeton/ASU models).

MacAyeal, D. R. (1993). Binge/purge oscillations of the Laurentide Ice Sheet. Paleoceanography, 8(6), 775–784.

Malhotra, R., Volk, K., Wang, X. (2016). Orbital clustering in the distant solar system. The Astrophysical Journal Letters, 824(2), L22.

Marcott, S. A., et al. (2013). A reconstruction of regional and global temperature for the past 11,300 years. Science, 339, 1198–1201. DOI: 10.1126/science.1228026

Marcott, S. A., et al. (2011). Ice-shelf collapse from subsurface warming as a trigger for Heinrich events. PNAS, 108(33), 13415–13419.

Marsden, B. G., Williams, J. G. (2008). Catalogue of Cometary Orbits 2008. CBAT.

Matney, M. J. (2025). The Star of Bethlehem the comet of 5 BCE. Journal of the British Astronomical Association, 135(6), 330-338.

McCormick, M., et al. (2012). Climate change during and after the Roman Empire. Journal of Interdisciplinary History, 43, 169–220.

Méndez, A. et al. (2025). "Arecibo Wow! II: Revised Properties of the Wow! Signal from Archival Ohio SETI Data" https://arxiv.org/abs/2508.10657

Migowski, C., et al. (2004). Reconstruction of Holocene Dead Sea level changes. Earth and Planetary Science Letters, 222, 301–314.

Mura, A., et al. (2009). The sodium exosphere of Mercury: Comparison between observations during Mercury's transit and model results. *Icarus*, 200(1), 1–11. https://doi.org/10.1016/j.icarus.2008.11.022

Mustill, A. J., et al. (2016). Capturing rogue planets. *Monthly Notices of the Royal Astronomical Society*, 460(1), 1. https://doi.org/10.1093/mnras/stw1004

MPC2025, IAU Minor Planet Center (2025). Discovery announcement of 3I/ATLAS. *IAU Circulars*. https://www.minorplanetcente Interstellar List

Nakajima, M., et al. (2026). Hidden magma oceans could shield rocky exoplanets. Nature Astronomy.

Napier, W. M. (2010). Palaeolithic extinctions and the Taurid Complex. Monthly Notices of the Royal Astronomical Society, 405(3), 1901-1906.

Oort, J. H. (1950). The structure of the cloud of comets surrounding the Solar System. Bulletin of the Astronomical Institutes of the Netherlands, 11, 91–110.

Owen, J. E. (2019). Atmospheric escape and the evolution of close-in exoplanets. *Annual Review of Earth and Planetary Sciences*, 47, 67–94. https://doi.org/10.1146/annurev-earth-053018-060246

Pankenier, D. W. (2013). Astrology and cosmology in early China. Cambridge University Press.

Peale, S. J., et al. (1979). Melting of Io by tidal dissipation. *Science*, 203(4383), 892–894. https://doi.org/10.1126/science.203.4383.8

Pingré, A. G. (1783–1784). Cometographie ou Traite Historique et Theorique des Cometes. Imprimerie Royale.

Potter, A. E., et al. (2002). The sodium tail of Mercury. *Meteoritics & Planetary Science*, 37(9), 1165–1172. https://doi.org/10.1111 5100.2002.tb00941.x

Rackham, H. (1938). Pliny: Natural History, Volume I. Harvard University Press.

Ramsey, J. T. (2006). A Descriptive Catalogue of Greco-Roman Comets from 500 B.C. to A.D. 400. Syllecta Classica, 17, 1–242.

Ramsey, J. T., Licht, A. L. (1997). The comet of 44 B.C. and Caesar's funeral games. Scholars Press.

Rappaport, S., et al. (2014). Dust clouds around Kepler stars. *Astrophysical Journal*, 789(2), 144. https://doi.org/10.1088/0004-637X/789/2/144

Ross, M. N., & Schubert, G. (1989). Volcanism on Io. *Icarus*, 79(1), 3–22. https://doi.org/10.1016/0019-1035(89)90102-0

Sagan, C., & Khare, B. N. (1979). Tholins: Organic chemistry of interstellar grains and gas. *Nature*, 277(5692), 102–107. https://doi.org/10.1038/277102a0

Sekanina, Z. (2002). Split comets. In Comets II (pp. 667–688). University of Arizona Press.

Sigl, M., et al. (2015). Timing and climate forcing of volcanic eruptions for the past 2,500 years. Nature, 523, 543–549. Siraj, A. (2023). Capture of interstellar objects and rogue planets. *The Astrophysical Journal Letters*, 945(1), L1. https://doi.org/10.3847/2041-8213/acb4f0

Siraj, A., Chyba, C. F., Tremaine, S. (2025). Orbit of a Possible Planet X. The Astrophysical Journal, 978(2), 139. DOI: 10.3847/1538-4357/ad9a41

Steinhilber, F., et al. (2012). Total solar irradiance during the Holocene. PNAS, 109(16), 5967–5971. DOI: 10.1073/pnas.112011510

Stephenson, F. R. (2002). Historical Supernovae and their Remnants. Oxford University Press.

Stern, S. A., et al. (2015). The Pluto system: New Horizons results. Science, 350(6258). DOI: 10.1126/science.aad1815

Sweatman, M. B., Tsikritsis, D. (2017). Decoding Göbekli Tepe with archaeoastronomy. Mediterranean Archaeology and Archaeometry, 17(1), 233-250.

Tachinami, C., et al. (2011). The role of rotation in the evolution of dynamo-generated magnetic fields in Super Earths. *Icarus*, 211(1), 818–829. https://doi.org/10.1016/j.icarus.2010.09.017

Thomas, N., et al. (2004). The morphological diversity of comet 67P/Churyumov-Gerasimenko. *Science*, 347(6220), aaa0440. https://doi.org/10.1126/science.aaa0440

Usoskin, I. G. (2017). A history of solar activity over millennia. Living Reviews in Solar Physics, 14, 3. DOI: 10.1007/s41116-017-0006-9

Valencia, D., et al. (2007). Radius and structure models of the first super-Earth planet. The Astrophysical Journal, 656(1), 545–551. DOI: 10.1086/509800

van Lieshout, R., et al. (2014). The disintegrating planetary system around WD 1145+017. *Monthly Notices of the Royal Astronomical Society*, 443(3), 2284–2295. https://doi.org/10.1093/mnras/stu1289

Vesper, J., Mason, P. A. (2017). Simulation of Rogue Planet Encounters: Is Planet 9 a Captured Rogue? AAS Meeting Abstracts / Astronomy Astrophysics.

Vesper, O., & Mason, P. (2017). Dynamical capture of rogue planets. *Astronomy & Astrophysics*, 598, A1. https://doi.org/10.1051/0 6361/201629589

Weingarten, M., Ge, S., Zohar, M. (2014). A paleoseismic record of earthquakes for the Dead Sea Transform... BSSA, 104(3), 1329–1347.

Wick, L., Tinner, W. (1997). Vegetation changes and timberline fluctuations in the Central Alps. Arctic and Alpine Research, 29(4), 445-458.

Williams, D. M., & Pollard, D. (2002). Earth-like worlds on eccentric orbits: Excursions beyond the habitable zone. *International Journal of Astrobiology*, 1(1), 61–69. https://doi.org/10.1017/S1473550402001090

Williams, J. B. P. (2012). An early first-century earthquake in the Dead Sea. International Geology Review, 54(10), 1219–1228.

Yeomans, D. K. (1994). A review of comet astrometry: 1801–1993. ACM 1993, Kluwer.

Zeng, L., et al. (2016). Growth model interpretation of planet size distribution. *Proceedings of the National Academy of Sciences*, 113(18), 5104–5109. https://doi.org/10.1073/pnas.1517369113

Zuluaga, J. I., & Cuartas, P. A. (2012). The role of rotation in the evolution of dynamo-generated magnetic fields in Super Earths. *Icarus*, 217(1), 88–102. https://doi.org/10.1016/j.icarus.2011.10.014